Monthly Notices
of the
ROYAL ASTRONOMICAL SOCIETY

MNRAS **459,** 3432–3446 (2016)
Advance Access publication 2016 April 14

doi:10.1093/mnras/stw869

Massive black hole binaries from runaway collisions: the impact of metallicity

Michela Mapelli[1,2]★

[1]*INAF–Osservatorio Astronomico di Padova, Vicolo dell'Osservatorio 5, I-35122, Padova, Italy*
[2]*INFN, Milano Bicocca, Piazza della Scienza 3, I-20126 Milano, Italy*

Accepted 2016 April 12. Received 2016 April 12; in original form 2016 February 20

ABSTRACT

The runaway collision scenario is one of the most promising mechanisms to explain the formation of intermediate-mass black holes (IMBHs) in young dense star clusters. On the other hand, the massive stars that participate in the runaway collisions lose mass by stellar winds. In this paper, we discuss new *N*-body simulations of massive (6.5×10^4 $M_\odot$) star clusters, in which we added upgraded recipes for stellar winds and supernova explosion at different metallicity. We follow the evolution of the principal collision product (PCP), through dynamics and stellar evolution, till it forms a stellar remnant. At solar metallicity, the mass of the final merger product spans from few solar masses up to ∼30 $M_\odot$. At low metallicity (0.01–0.1 $Z_\odot$) the maximum remnant mass is ∼250 $M_\odot$, in the range of IMBHs. A large fraction (∼0.6) of the PCPs are not ejected from the parent star cluster and acquire stellar or black hole (BH) companions. Most of the long-lived binaries hosting a PCP are BH–BH binaries. We discuss the importance of this result for gravitational wave detection.

Key words: gravitational waves – methods: numerical – stars: black holes – stars: kinematics and dynamics – stars: mass-loss – galaxies: star clusters: general.

1 INTRODUCTION

Young (<100 Myr) dense ($\gtrsim 10^3$ $M_\odot$ pc^{-3}) star clusters (YDSCs) are one of the most crowded nurseries of stars in the local Universe (Lada & Lada 2003). Given its high central density, the core of a YDSC is the ideal environment for extreme dynamical interactions between stars, including stellar collisions, which are unlikely to occur in the galactic field (see Portegies Zwart, McMillan & Gieles 2010 for a review). Stellar collisions are enhanced when the core of the YDSC undergoes a gravothermal instability (Freitag, Gürkan & Rasio 2006b), because the central density can grow by orders of magnitude. Most collisions are triggered by three-body encounters (i.e. close encounters between a star and a binary system, Heggie 1975), in the sense that they occur preferentially between one of the members of a binary system and a stellar intruder (Gaburov, Gualandris & Portegies Zwart 2008b).

The most massive objects in a YDSC are more likely to undergo stellar collisions, because dynamical friction brings them to the YDSC core in few Myr (Gaburov et al. 2008b). Moreover, they are particularly efficient in forming binary systems through close encounters of three single stars and through dynamical exchanges (Hills 1976; Hills & Fullerton 1980; Hills 1989, 1991, 1992; MacLeod, Trenti & Ramirez-Ruiz 2016). Thus, the most massive objects may experience multiple collisions (Portegies Zwart et al. 1999): the larger their mass becomes after a collision, the higher the probability that they participate in a further collision, unless they are dynamically ejected by the YDSC. According to the runaway collision scenario (Colgate 1967; Sanders 1970; Quinlan & Shapiro 1990; Portegies Zwart et al. 1999; Ebisuzaki et al. 2001; Portegies Zwart & McMillan 2002), a massive object experiencing multiple collisions can become a very massive blue straggler star (with mass $\gg$100 $M_\odot$) and then it might collapse to an intermediate-mass black hole (IMBH), i.e. a black hole (BH) with mass larger than expected for stellar-mass BHs (∼10^2 $M_\odot$, Spera, Mapelli & Bressan 2015), but smaller than $\lesssim 10^5$ $M_\odot$.

The evolution of the collision product is one of the main open questions of the runaway merger scenario. A very massive merger product may lose mass by stellar winds (Glebbeek et al. 2009). At the end, the merger product may explode as a supernova (SN, Portegies Zwart & van den Heuvel 2007; Pan, Loeb & Kasen 2012; van den Heuvel & Portegies Zwart 2013), or it may preserve enough mass to collapse to a BH directly (Fryer 1999; Heger et al. 2003; Fryer et al. 2012; Spera et al. 2015). The mass of the final remnant is in the IMBH mass range only if mass-loss by stellar winds is moderate and only if direct collapse takes place.

Several direct *N*-body simulations (Portegies Zwart & McMillan 2002; Moeckel & Clarke 2011) and Monte Carlo simulations

★E-mail: michela.mapelli@oapd.inaf.it

(Gürkan, Fregeau & Rasio 2006; Goswami et al. 2012) investigating the runaway merger do not include prescriptions for stellar evolution, mass-loss by stellar winds and SN explosions. A number of studies adopt models for stellar evolution and/or approximate recipes for mass-loss and SNe (Portegies Zwart et al. 1999, 2004; Gürkan, Freitag & Rasio 2004; Freitag, Rasio & Baumgardt 2006a; Freitag et al. 2006b; Arca-Sedda 2016). Only few authors include a detailed treatment of mass-loss during the collision (Gaburov, Lombardi & Portegies Zwart 2008a, 2010) and afterward, as a consequence of stellar winds (Glebbeek et al. 2009, 2013; Banerjee, Kroupa & Oh 2012).

Hydrodynamical simulations of the merger of massive stars show that up to ∼25 per cent of the total mass of the colliding stars might be lost during the merger (Gaburov et al. 2010). Moreover, all previous studies including recipes for stellar evolution agree that the massive merger product is expected to lose most of its mass by stellar winds at solar metallicity. Lower metallicity environments may be the most important ones for the formation of IMBHs (Mapelli, Colpi & Zampieri 2009; Belczynski et al. 2010; Spera et al. 2015), since stellar winds are less effective in metal-poor stars (Kudritzki, Pauldrach & Puls 1987; Vink, de Koter & Lamers 2001; Kudritzki 2002).

However, only few studies consider metal-poor clusters (e.g. Glebbeek et al. 2009). Moreover, the evolutionary models of massive and very massive stars have been deeply revised in the last few years (e.g. Vink et al. 2001; Vink & de Koter 2005; Yungelson et al. 2008; Tang et al. 2014; Chen et al. 2015 and references therein). Glebbeek et al. (2009) is one of the few studies that use up-to-date metallicity-dependent stellar evolution recipes (stellar winds are based on Vink et al. 2001 and Vink & de Koter 2005). However, Glebbeek et al. (2009) include these stellar-wind recipes *a posteriori*, in *N*-body simulations that were run without stellar evolution (or with older models of stellar evolution at solar metallicity). This procedure introduces a bias, since the mass-loss of the merger product affects the probability that the merger product undergoes further collisions with other stars. Moreover, stellar winds affect the gravothermal instability phase of the host star cluster: they make the potential well of the core shallower, reducing the amount of kinetic energy that must be provided by three-body encounters to reverse the core collapse (Trani, Mapelli & Bressan 2014). As a consequence, three-body encounters and stellar collisions are less effective, if stellar winds are included (Mapelli & Bressan 2013).

In this paper, we study the runaway collision scenario through direct *N*-body simulations of YDSCs with different metallicity, adopting upgraded recipes for metallicity-dependent stellar evolution and mass-loss by stellar winds (Mapelli et al. 2013). We investigate the evolution of the principal collision product (PCP), defined as the product of the first collision that occurs in a simulated YDSC, till it becomes a stellar remnant. Our main goal is to study whether (or not) the PCP acquires companions through dynamical processes and what are the properties of such PCP binaries. We focus on the importance of PCP binaries for the emission of gravitational waves (GWs) in YDSCs, in light of the recent first direct detection of GWs by Advanced LIGO (Abbott et al. 2016a,b; The LIGO Scientific Collaboration & the Virgo Collaboration 2016).

This paper is organized as follows. In Section 2, we describe the methods used in this paper and the simulation setup. Our results are presented in Section 3. In Section 4 we discuss the implications of our findings, focusing on GW detections. Our conclusions are summarized in Section 5.

2 METHODS: *N*-BODY SIMULATIONS

2.1 *N*-body and stellar evolution

We ran a set of 30 direct *N*-body simulations of YDSCs using the STARLAB public software environment (Portegies Zwart et al. 2001). KIRA, the direct *N*-body integrator included in STARLAB, implements a Hermite fourth-order integration algorithm (Makino & Aarseth 1992) and a neighbours–perturbers scheme to ensure an accurate integration of tight binaries and multiple systems. We included stellar and binary evolution, using the modified version of STARLAB described in Mapelli et al. (2013). Stars evolve in radius, temperature and luminosity at different metallicities, based on the polynomial fitting formulae by Hurley, Pols & Tout (2000). The original fitting formulae of Hurley et al. (2000) were developed for stars with a maximum mass of 100 $M_\odot$. In our code, we extrapolate them for higher masses (Mapelli et al. 2013). To avoid unphysical results, we request that the values of the radius of single stars are consistent with PARSEC stellar evolution tracks (Bressan et al. 2012; Tang et al. 2014; Chen et al. 2015) for stars with mass >100 $M_\odot$, as implemented in our new population synthesis code SEVN (Spera et al. 2015).

A treatment of stellar winds is included both for main-sequence (MS) and post-MS stars. Massive MS stars lose mass based on the metallicity-dependent fitting formulae described in Vink et al. (2001). The mass-loss rate of luminous blue variable (LBV) stars (i.e. stars whose luminosity L and radius R satisfy the requirement that $L/L_\odot > 6 \times 10^5$ and $10^{-5}\,(R/R_\odot)\,(L/L_\odot)^{0.5} > 1.0$, Humphreys & Davidson 1994) is $\dot{M} = f_{\rm LBV} \times 10^{-4}$ $M_\odot$ yr^{-1}, where $f_{\rm LBV} = 1.5$ (Belczynski et al. 2010). Wolf–Rayet (WR) stars undergo a mass-loss rate by stellar winds defined by $\dot{M} = 10^{-13}(L/L_\odot)^{1.5}\,(Z/Z_\odot)^{\beta}$ $M_\odot$ yr^{-1}, where $\beta = 0.86$ (Hamann & Koesterke 1998; Vink & de Koter 2005; Belczynski et al. 2010). Stellar winds in asymptotic giant branch (AGB) stars are modelled as in the standard version of STARLAB (Portegies Zwart & Verbunt 1996), and do not depend on metallicity.

We assume that the mass lost by stellar winds and SNe is immediately removed from the simulation. This assumption is correct for SN ejecta and also for the winds of massive stars, which are expected to move fast ($\gtrsim$1000–2000 km s^{-1}, Vink & de Koter 2005; Muijres et al. 2012) with respect to the escape velocity of the simulated YDSCs (∼20–25 km s^{-1}).

The formation of stellar remnants is implemented as described in Mapelli et al. (2013). In particular, BH masses at various metallicities follow the distribution described in fig. 1 of Mapelli et al. (2013) (see also Fryer 1999; Fryer & Kalogera 2001; Fryer et al. 2012). If the final mass $m_{\rm fin}$ of the progenitor star (i.e. the mass bound to the star immediately before the collapse) is >40 $M_\odot$, we assume that the SN fails and that the star collapses quietly to a BH. The requirement that $m_{\rm fin} > 40$ $M_\odot$ implies that only stars with zero-age MS (ZAMS) mass $\gtrsim 80$ and $\gtrsim$100 $M_\odot$, can undergo a direct collapse at $Z = 0.01$ and 0.1 $Z_\odot$, respectively. The mass of a BH born from direct collapse is similar to the final mass of the progenitor star. Thus, BHs with mass up to ∼80 $M_\odot$ (∼40 $M_\odot$) can form if the metallicity of the progenitor is $Z \sim 0.01$ $Z_\odot$ ($Z \sim 0.1$ $Z_\odot$). Spera et al. (2015) suggest that the threshold for direct collapse is even lower ($m_{\rm fin} \sim 30$ $M_\odot$) and that the maximum mass of a BH for a given metallicity can be even higher than discussed in Mapelli et al. (2013), but these predictions cannot be implemented in our simulations because they still lack a treatment of binary evolution and its effects on the BH mass.

Neutron stars (NSs) are assumed to receive a natal kick drawn from the distribution of Hartman (1997). BHs that form from quiet collapse are assumed to receive no natal kick (Fryer et al. 2012). For BHs that form from an SN explosion, the natal kicks were drawn from the same distribution as NSs but scaled as $m_{\rm NS}/m_{\rm BH}$ (where $m_{\rm NS} = 1.3$ M$_\odot$ is the typical mass of a NS, while $m_{\rm BH}$ is the mass of the considered BH), to preserve linear momentum.

The evolution of binaries is implemented as described in Portegies Zwart & Verbunt (1996) and Portegies Zwart et al. (2001): we include mass transfer by stellar winds, mass transfer by Roche lobe overflow, magnetic braking, energy and angular-momentum loss due to GW emission (Peters 1964), tidal circularization, common envelope (following the formalism proposed by Webbink 1984 and de Kool 1990, with binding energy coefficient $\lambda = 0.5$ and efficiency coefficient $\alpha_{\rm CE} = 1.0$).

If two stars approach each other by less than $d = (r_1 + r_2)$, where r_1 and r_2 are the radius of the first and second star, respectively, they are merged to a single particle with mass equal to the total mass of the progenitor. This is an optimistic assumption, since it does not consider the relative velocity between the two stars and it assumes that no mass is lost during the merger. While on the MS, the merger product is rejuvenated by a rejuvenation fraction (Meurs & van den Heuvel 1989; Portegies Zwart et al. 1999)

$$f_{\rm rej}(m_1, m_2) = \frac{m_1}{m_1 + m_2} \frac{\tau_{\rm MS}(m_1 + m_2)}{\tau_{\rm MS}(m_1)}, \quad (1)$$

where m_1 and $\tau_{\rm MS}(m_1)$ are the mass and the MS lifetime of the most massive among the two colliding stars, m_2 is the mass of the other colliding star, and $\tau_{\rm MS}(m_1 + m_2)$ is the MS lifetime of a star with mass equal to the mass of the collision product. The new age of the collision product is $t(m_1 + m_2) = f_{\rm rej}(m_1 + m_2)\, t(m_1)$, where $t(m_1)$ is the age of the first progenitor star at the time of the collision. For collisions of post-MS stars the rejuvenation is calculated with a similar formula, in which we substitute $\tau_{\rm MS}$ with the lifetime of the corresponding evolutionary stage (e.g. $\tau_{\rm SG}$ for a sub-giant star), while $t(m_1)$ indicates the time the star of mass m_1 has already spent on its current evolutionary stage (e.g. the time spent in the sub-giant branch), instead of the total stellar age (see Portegies Zwart et al. 2001 for details). Rejuvenation of an MS star is generally more conspicuous than rejuvenation of post-MS stars, since the time a star spends in post-MS evolutionary stages is $<1/10$ of its entire lifetime.

2.2 Initial conditions and simulations grid

We simulate 30 YDSCs with $N = 10^5$ particles each (in our simulations each particle is a single star), corresponding to an average total mass $M_{\rm TOT} \sim 6.5 \times 10^4$ M$_\odot$. The YDSCs are modelled as King models (King 1966) with virial radius $r_{\rm v} = 1$ pc, core radius $r_{\rm c} \sim 0.05$ pc, half-mass radius $r_{\rm hm} \sim 0.98$ pc, and central dimensionless potential $W_0 = 9$ (Fig. 1). These values are reminiscent of the YDSCs in the Milky Way (Portegies Zwart et al. 2010), and are not as extreme as the ones adopted in previous studies (e.g. Gaburov et al. 2008b). We generate star masses according to a Kroupa initial mass function (IMF, Kroupa 2001) with minimum mass $m_{\rm low} = 0.1$ M$_\odot$ and maximum mass $m_{\rm up} = 150$ M$_\odot$.

We do not include primordial binaries. These are the most computationally expensive ingredient, but should be accounted for in future work, because a high binary fraction is observed in young star clusters (e.g. Li, de Grijs & Deng 2013). If there are no primordial binaries, binaries can form through close encounters of three single stars, during which two stars transfer sufficient kinetic energy to the third one to become bound to each other, while the third star flies away.

We consider star clusters at three different metallicities: $Z = 0.02$, 0.002 and 0.0002. Assuming $Z_\odot = 0.02$, this means that we consider star clusters with metallicity $Z = 1$, 0.1, and 0.01 Z$_\odot$, respectively. We simulate 10 different realizations for each of these metallicities (Table 1), to filter out stochastic fluctuations.

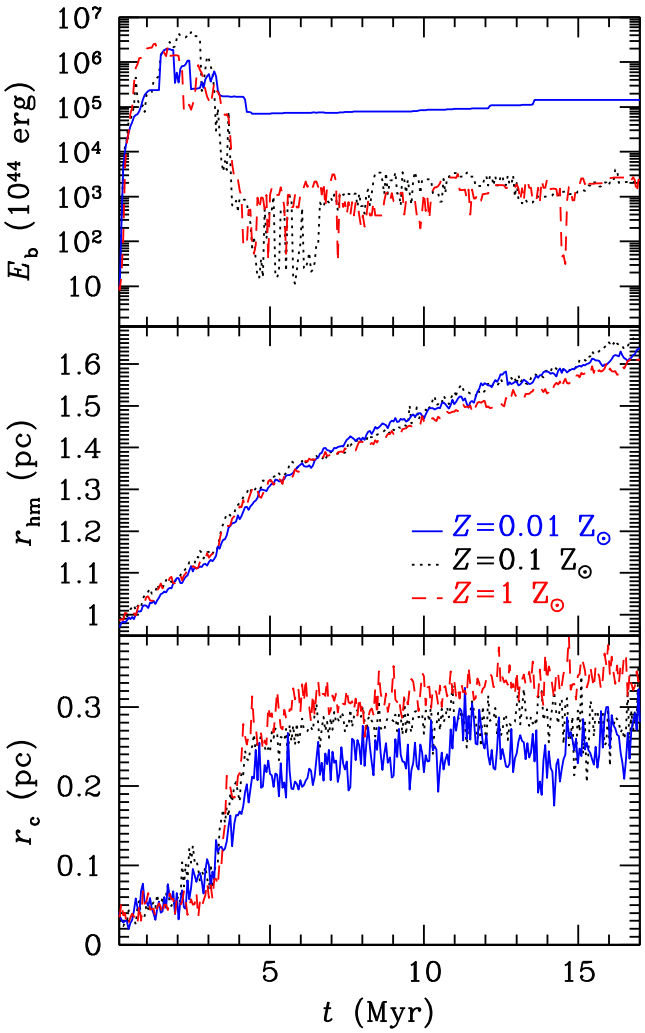

Figure 1. Bottom panel: evolution of the core radius $r_{\rm c}$ as a function of time; central panel: evolution of the half-mass radius $r_{\rm hm}$ as a function of time; top panel: evolution of the total binding energy stored in binaries $E_{\rm b}$ as a function of time. Each line is the median value of 10 realizations of the same YDSC model. Red dashed line: $Z = 1$ Z$_\odot$; black dotted line: $Z = 0.1$ Z$_\odot$; blue solid line: $Z = 0.01$ Z$_\odot$.

Table 1. Initial conditions of the N-body simulations.

$N_{\rm runs}$	$Z/{\rm Z}_\odot$	N_*	$r_{\rm v}$/pc	W_0
10	1.0	10^5	1	9
10	0.1	10^5	1	9
10	0.01	10^5	1	9

Column 1: number of N-body realizations; column 2: metallicity; column 3: number of particles (N_*); column 4: virial radius $r_{\rm v}$; column 5: dimensionless central potential.

We simulate each YDSC for $t = 17$ Myr. At this time, the stage of runaway merger has already completed and binaries including BHs have already formed.

In our simulations, we do not include the contribution of the tidal field of the host galaxy, because this would add more parameters to deal with. Milky Way YDSCs are observed both near the Galactic Centre (Arches, Quintuplet) and close to the Sun (Trumpler 14, Portegies Zwart et al. 2010). Accounting for various tidal fields would require a much larger sample of simulations.

Moreover, the Galactic tidal field is not sufficiently strong to disrupt the YDSCs for the entire duration of our simulations (17 Myr), even for YDSCs close to the Galactic Centre (Gieles & Portegies Zwart 2011).

3 RESULTS

3.1 Structural evolution of the YDSCs and formation of binaries

Fig. 1 shows the evolution of the core radius r_c (bottom panel) and the half-mass radius r_{hm} (central panel) of the simulated YDSCs as a function of time for the three different metallicities (each line is the median value of r_c and r_{hm} over 10 runs with the same metallicity, to filter our stochastic fluctuations). Both the core and the half-mass radius start expanding rapidly at time $t \sim 3$ Myr.

The impact of mass-loss by stellar winds and SNe on the evolution of r_c and r_{hm} has already been discussed in Mapelli & Bressan (2013) and Trani et al. (2014). Here, we recall that massive stars ($>30\,M_\odot$) lose most of their mass by stellar winds in the first ∼2–6 Myr, while most SNe occur between ∼3 and ∼50 Myr. At low-metallicity ($Z \leq 0.1\,Z_\odot$) the most massive stars are allowed to collapse to BH without SN.

The mass ejected by stellar winds and SNe is lost from the YDSC, making the potential well shallower. Thus, mass-loss contributes to drive the expansion of the core (Fig. 1). Three-body encounters, which transfer kinetic energy to stars, are the other main driver of the expansion of the core. The contribution of stellar winds is more important at high metallicity; in fact, the core radius of metal-rich clusters expands more than that of metal-poor clusters (Fig. 1).

The top panel of Fig. 1 shows the total binding energy of binaries E_b, i.e. the sum of the binding energies of all binaries in a YDSC at a given time. The binding energy of a binary in Fig. 1 drops to zero only if the binary merges or becomes unbound (because of SN kicks or three-body encounters). Binaries that are ejected from the YDSC are not removed from Fig. 1.

Binaries form very rapidly at the beginning of the simulations, regardless of the metallicity. The formation of binaries is driven by encounters of three single stars.

The reason why binary formation is so efficient in the first ∼5 Myr can be explained as follows. The initial half-mass relaxation time-scale of our YDSCs is (Portegies Zwart et al. 2010)

$$t_{rlx} \sim 50\,\mathrm{Myr} \left(\frac{M_{TOT}}{6.5\times10^4\,M_\odot}\right)^{1/2} \left(\frac{r_v}{1\,\mathrm{pc}}\right)^{3/2} \left(\frac{\langle m\rangle}{1\,M_\odot}\right)^{-1}, \quad (2)$$

where M_{TOT} is the total mass of the YDSC, r_v is the virial radius, and $\langle m\rangle$ is the average mass of a star. Thus, the dynamical friction time-scale of a star of mass m is

$$t_{DF}(m) \sim \frac{\langle m\rangle}{m}\, t_{rlx} \sim 2\,\mathrm{Myr} \left(\frac{m}{25\,M_\odot}\right)^{-1}. \quad (3)$$

This means that the massive stars segregate to the core of the YDSC in few Myr. Thanks to the high density of the core, the massive stars interact with each other and effectively build binaries, before undergoing SN explosion or directly collapsing to a BH.

At $t > 5$ Myr, the binary binding energy of YDSCs with metallicity $Z = 0.01\,Z_\odot$ is much higher (more than one order of magnitude) than that of YDSCs with $Z = 0.1, 1\,Z_\odot$. This large difference comes from the fact that metal-poor binaries can be significantly more massive at late epochs, because they lose less mass by stellar winds and collapse into more massive BHs than metal-rich systems. Moreover, binaries tend to live for a longer time at low metallicity, because BHs born from direct collapse receive no natal kick, and, if they are members of a binary, the binary is not destroyed by the kick.

3.2 Mass evolution of principal collision products (PCPs)

In each simulated YDSC, we identify the first two stars that have a genuine collision (we exclude mergers in contact binaries triggered by stellar evolution) and we track the subsequent history of this first collision product (hereafter, the principal collision product, PCP). Thus, we have a sample of 10 PCPs for each simulated metallicity (in Appendix A, we also examine some of the properties of the other collision products).

According to our definition, we consider as 'genuine collisions' all collisions that are not triggered uniquely by stellar or binary evolution. Thus, the collision might occur between two single stars, or between a single star and the member of a binary, or between two members of a binary that was dynamically perturbed by the dynamical encounter with a third body. We find no PCP born from the collision of two single stars. All PCPs originate from encounters that involve a binary, confirming that binary interactions are very important for the runaway merger (Gaburov et al. 2008b). Most of PCPs form from the collision between a member of a binary and a third star in a three-body encounter (70, 60, and 50 per cent at $Z = 1$, 0.1 and 0.01 $Z_\odot$, respectively). The remaining PCPs form from the collision between the two former members of a binary, and the collision is triggered by a three-body encounter. Figs 2–4 show the mass evolution of the PCP at the three considered metallicities, distinguishing between PCPs that are ejected before the end of the simulation and PCPs that are not. Symbols in these figures mark the time of each collision. In all set of runs, 40 per cent of the PCPs are ejected from the parent YDSC. The retained PCPs undergo on average ∼2.9 collisions during the entire simulations, whereas the ejected PCPs undergo only ∼1.5 collisions, because no collisions occur after they are ejected (we note however that in run n2 at $Z = Z_\odot$ the PCP undergoes 5 collisions before being ejected).

The average number of collisions is lower than previously reported by several authors (Portegies Zwart et al. 1999; Glebbeek et al. 2009). The main reasons are that (i) we include the contribution of stellar winds, which quench the core collapse and keep the central stellar density lower (Mapelli & Bressan 2013; Trani et al. 2014), and (ii) our simulated YDSCs have less extreme central densities than those assumed in previous studies. For example, the virial radii considered in Gaburov et al. (2008b) span from 0.05 to 0.75 times those assumed in our simulated YDSCs.

At solar metallicity (Fig. 2) the final mass of the PCP is always low ($\lesssim 30\,M_\odot$), because the PCP undergoes strong mass-loss by stellar winds. For example, the star that undergoes the largest number of collisions at $Z = Z_\odot$ (run n4) starts from a ZAMS mass of ∼136 $M_\odot$, collides for the first time with a binary system at $t \sim 1.2$ Myr, before mass-loss by stellar winds becomes

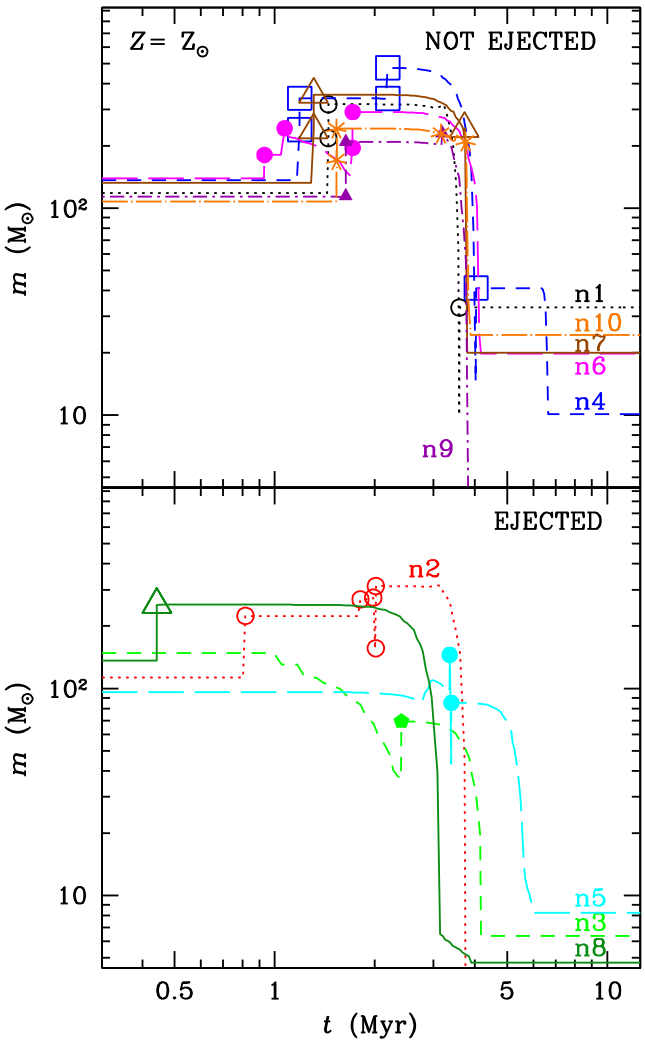

Figure 2. Mass evolution of PCPs in runs with metallicity $Z = Z_{\odot}$. Top panel: PCPs that are not ejected from the YDSC. Bottom panel: PCPs that are ejected from the YDSC. Each line corresponds to the evolution of a single PCP till the formation of the stellar remnant. Symbols mark single collisions in the evolution of a PCP. Dotted black line (with open circles): run n1; dotted red line (with open circles): run n2; dashed green line (with solid pentagons): run n3; dashed blue line (with open squares): run n4; long-dashed cyan line (with solid circles): run n5; long-dashed magenta line (with solid circles): run n6; solid brown line (with open triangles): run n7; solid dark green line (with open triangles): run n8; dot–dashed violet line (with solid triangles): run n9; dot–long-dashed orange line (with asterisks): run n10.

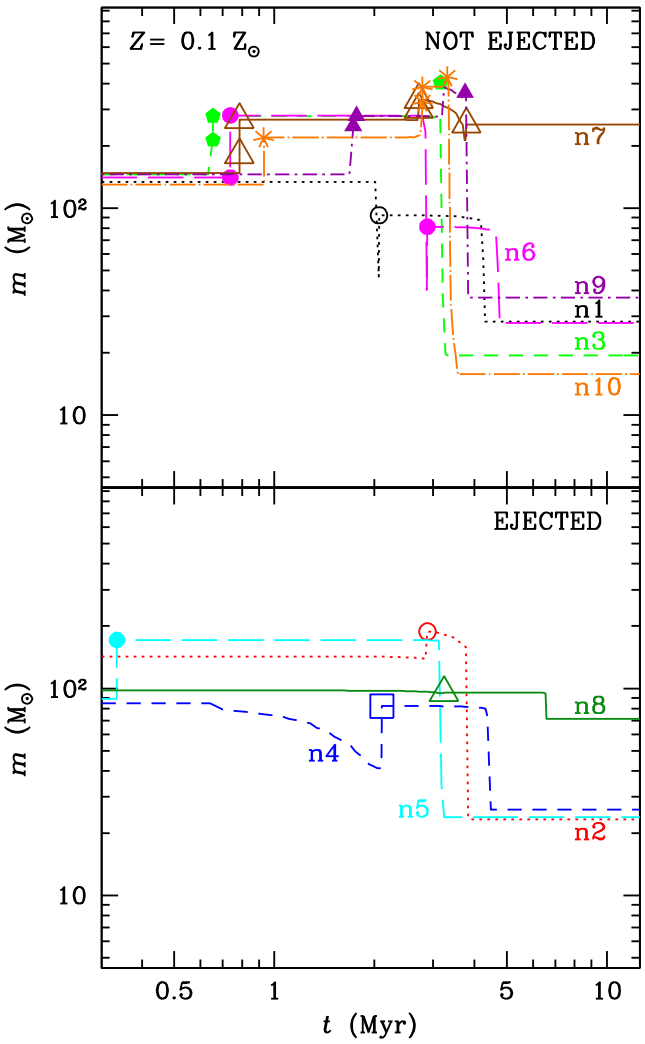

Figure 3. Same as Fig. 2 but for metallicity $Z = 0.1\ Z_{\odot}$.

important. Its mass becomes ∼340 $M_{\odot}$ and the object is rejuvenated according to equation (1). It undergoes a second collision at time $t \sim 2.16$ Myr, with another binary system (collisions with binary systems are frequent, because binary systems have a larger cross-section than single stars), and its mass rises up to ∼476 $M_{\odot}$. Right after this collision, stellar winds start to be important and the mass of the object drops fast, till it collides with one more object (another O-type object, with mass ∼41 $M_{\odot}$). The final merger product loses most of its mass by stellar winds, undergoes an SN explosion and becomes an ∼10 $M_{\odot}$ BH.

At lower metallicity (Figs 3 and 4) the situation is different, because stellar winds are less efficient. For example, the star that undergoes the largest number of collisions at $Z = 0.1\ Z_{\odot}$ (run n7) starts from a ZAMS mass of ∼148 $M_{\odot}$. It collides for the first time at $t = 0.8$ Myr (well before stellar winds become important) with a binary system, and reaches a mass of ∼268 $M_{\odot}$. It is rejuvenated according to equation (1). At ∼2.7 Myr it undergoes a further collision with another binary, and the mass of the PCP becomes ∼334 $M_{\odot}$. At this stage, the PCP is a very massive O-type star with an age ∼3 Myr: it suffers from stellar winds even if it is relatively metal-poor (it is a radiation pressure dominated object, anyway). At the end of the mass-loss phase it becomes a BH of ∼210 $M_{\odot}$ by direct collapse.

At $t \sim 3.8$ Myr, the BH collides one more time with a hyper-giant star (with mass ∼40 $M_{\odot}$). According to our simplified recipes, the entire mass of the hyper-giant star is swallowed by the BH, which becomes an ∼254 $M_{\odot}$ BH. A BH of ∼254 $M_{\odot}$ can be considered an IMBH.

We stress that a metallicity $Z = 0.1\ Z_{\odot}$ is low, but not dramatically so: this is the typical metallicity of several dwarf galaxies in the local Universe (Mapelli et al. 2010). We note that the most massive BHs in Figs 3 and 4 come from PCPs that undergo the last collision relatively late, when they would have started losing mass by stellar winds if they had not suffered a new collision. However, not all PCPs that undergo the last collision relatively late succeed in forming a massive BH, because the final mass of the BH depends on several ingredients (stellar winds, SN explosion) other than the dynamical encounters.

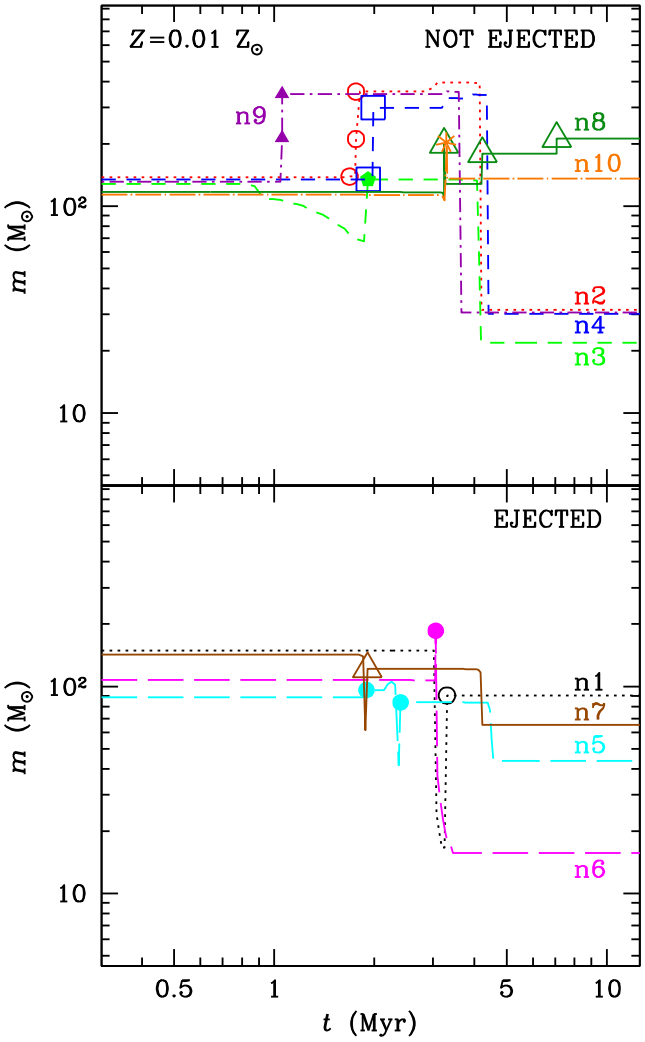

Figure 4. Same as Fig. 2 but for metallicity $Z = 0.01\ Z_{\odot}$.

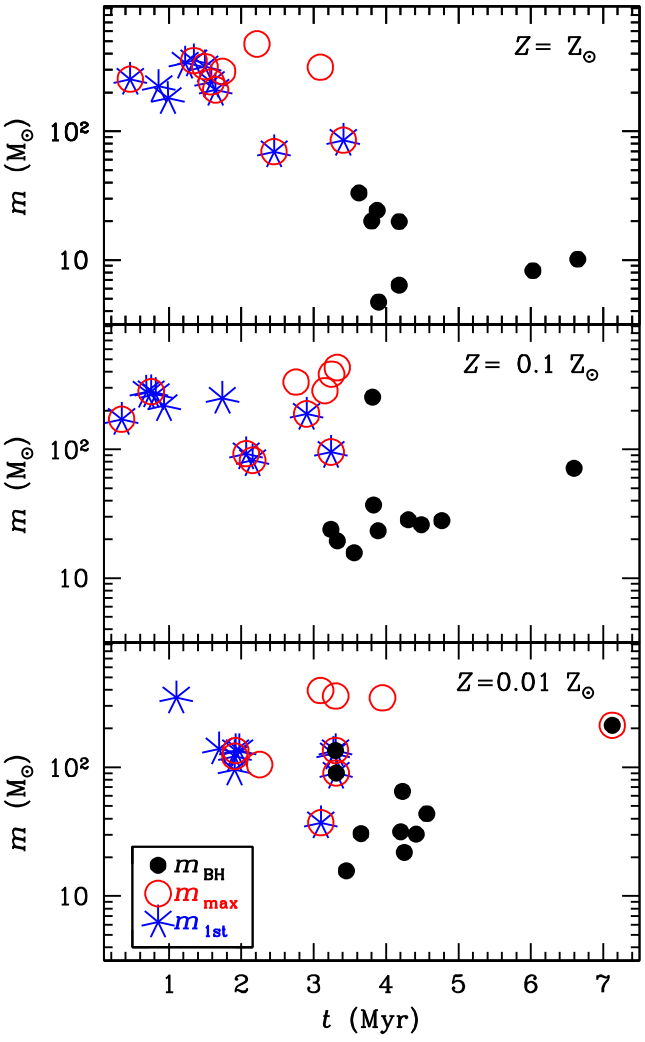

Figure 5. Mass of the PCP after the first collision (m_{1st}, blue asterisks), maximum mass of the PCP (m_{max}, red open circles) and mass of the BH generated by the PCP (m_{BH}, black solid circles) as a function of time, at solar metallicity (top), $Z = 0.1\ Z_{\odot}$ (centre) and $Z = 0.01\ Z_{\odot}$ (bottom).

One important caveat about Figs 2–4 is that the mass evolution of the PCP is sensitive to many physical processes, including (1) the rejuvenation induced by the merger, (2) mass transfer to a companion star, (3) the evolutionary stage of the colliding objects (MS or post-MS), and (4) the amount of fallback to the final BH.

There are several uncertainties and approximations in our treatment of these processes. For example, the rejuvenation of the merger product should be estimated accounting for the actual chemical mixing (Gaburov et al. 2008a). Moreover, it is unlikely that no mass is lost during the collision (Gaburov et al. 2010). Thus, the results depicted in Figs 2–4 should be regarded as rather optimistic.

Finally, Fig. 5 is a summary of the most important properties of the PCPs: for each PCP at each metallicity we show the mass after the first collision, the maximum mass ever reached, and the mass of the final remnant. In several cases, the mass reached after the first collision is also the maximum mass ever, because the PCP undergoes only one collision and/or because stellar winds prevent larger masses to be reached later on. For most PCPs, the maximum mass is $>100\ M_{\odot}$. In the most extreme cases $m_{max} \sim 300$–$500\ M_{\odot}$. This result is relevant for the observation of very massive stars in the local Universe (e.g. in the R136 star cluster, Crowther et al. 2010).

The mass of the remnant is the same as the maximum mass of the PCP only in three cases, all of them at $Z = 0.01\ Z_{\odot}$. At $Z = Z_{\odot}$ all BH masses are in the ∼5–30 $M_{\odot}$ range (there are even two objects that do not become BHs). At $Z = 0.1\ Z_{\odot}$ most BH masses are between ∼10 and ∼40 $M_{\odot}$, which is consistent with the BH mass we expect at this metallicity, given the stellar evolution recipes we adopt (Mapelli et al. 2013). However, there are two objects with mass 71 and 254 $M_{\odot}$, respectively, which can be considered in the IMBH mass range. At $Z = 0.01\ Z_{\odot}$, BH masses are between ∼10 and ∼70 $M_{\odot}$, which is, also in this case, the mass range that we expect at this metallicity, given the stellar evolution recipes we adopt. However, three BHs have mass above this range (90, 135 and 212 $M_{\odot}$), and can be considered IMBHs. Fig. 6 shows the number of stars that collide to form a PCP versus the maximum PCP mass (bottom panel) and versus the mass of the BH born from the PCP (top panel). In the bottom panel, there is a clear trend: the more stars collide, the higher the maximum mass of the PCP can be. There is a similar trend between the maximum PCP mass and the time when the first collision occurred (Fig. 7, bottom panel): the sooner the PCP starts building, the more massive it can become.

However, this trend does not persist if we look at the BH mass: the mass of the BH that forms from the PCP depends on neither the

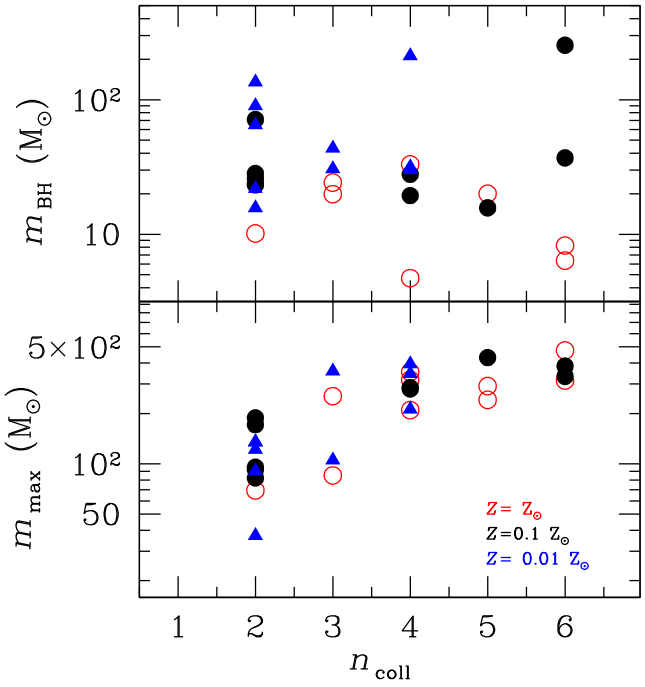

Figure 6. Number of stars that collide (n_{coll}) versus the maximum PCP mass (bottom panel) and versus the mass of the BH born from the PCP (top panel). Red open circles: $Z = 1\ Z_\odot$; black solid circles: $Z = 0.1\ Z_\odot$; blue solid triangles: $Z = 0.01\ Z_\odot$.

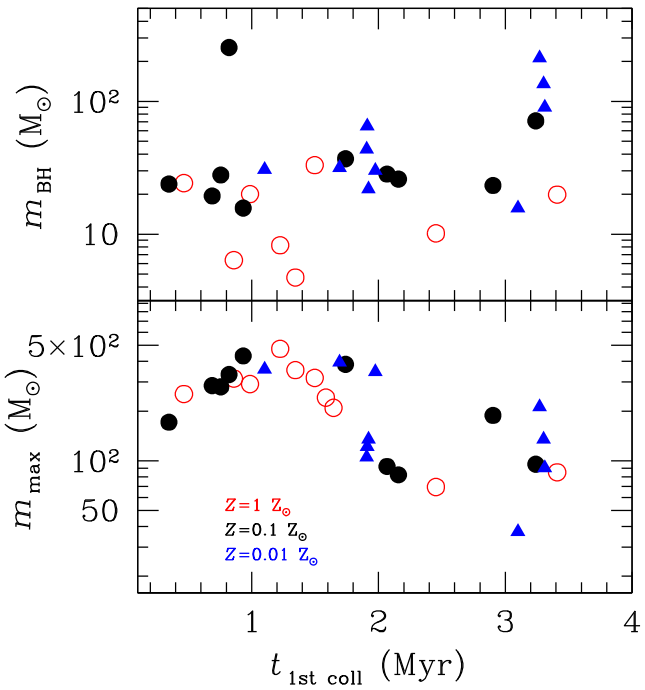

Figure 7. Time of the first collision ($t_{1st\,coll}$) versus the maximum PCP mass (bottom panel) and versus the mass of the BH born from the PCP (top panel). Red open circles: $Z = 1\ Z_\odot$; black solid circles: $Z = 0.1\ Z_\odot$; blue solid triangles: $Z = 0.01\ Z_\odot$.

number of stars that collide (Fig. 6, top panel) nor the time of the first collision (Fig. 7, top panel). This confirms that the mass of the remnant depends on the properties of the late evolution of the PCP (e.g. when the last collision occurs) rather than on the first collision and on the number of collisions. Overall, the masses of BHs born from PCPs span a large range of values, regardless of the number and time of collisions. This happens because the BH mass depends on many ingredients (stellar evolution, stellar winds and SN model) other than the dynamical evolution of the progenitor (Fryer et al. 2012; Mapelli et al. 2013; Spera et al. 2015).

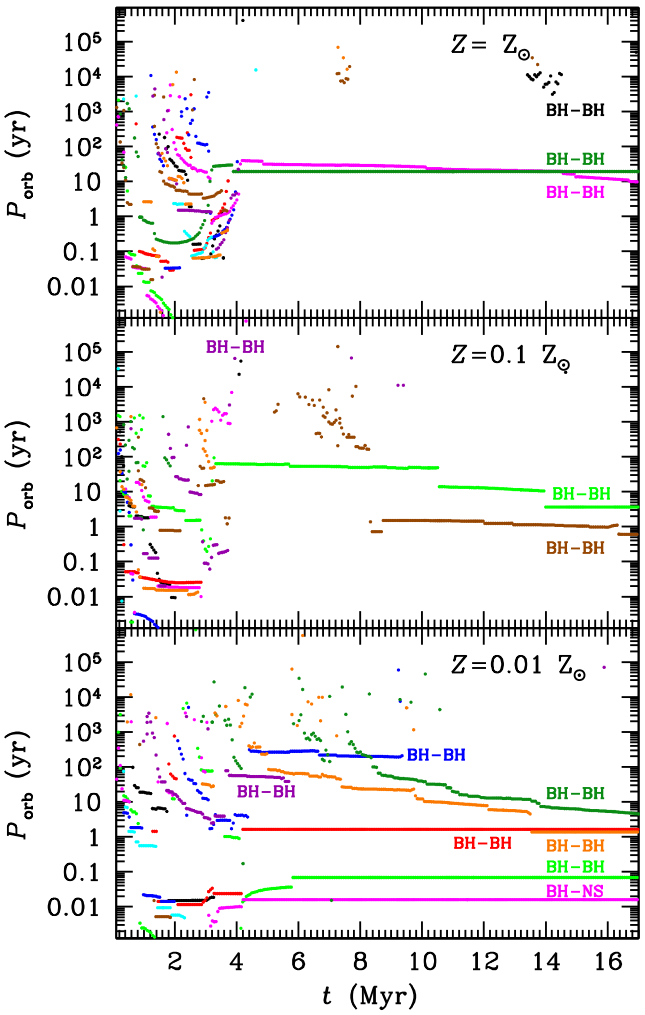

Figure 8. Period of the binary systems whose member is a PCP as a function of time. From top to bottom: $Z = Z_\odot$, $Z = 0.1\ Z_\odot$ and $Z = 0.01\ Z_\odot$. Each line is a single PCP. The labels 'BH–BH' and 'BH–NS' mark PCPs that are members of 'black hole–black hole' and 'black hole–neutron star' binaries, respectively. Colours associated with the single runs are the same as in Figs 2–4.

3.3 PCP binary systems

In this section, we study whether the PCP acquires a companion and evolves in a binary system. This aspect has not been highlighted in previous papers, but is extremely important for several reasons. First, the most massive stars in the local Universe are often found in binary systems (Crowther et al. 2010). Moreover, if the PCP ends its life as a BH that is more massive than most of the other BHs in the YDSC, its efficiency in acquiring companions (and especially compact-object companions) is higher: this is important for GW observations.

Fig. 8 shows the period of the binary hosting the PCP (when the PCP is member of a binary) as a function of time, for the entire duration of the simulations. During the early stages

Table 2. Properties of the stable PCP binaries at the end of the simulations.

Run	$Z/Z_\odot$	$M_{PCP}/M_\odot$	$M_{co}/M_\odot$	$m_c/M_\odot$	P_{orb}/yr	e	Type	Ejected?	$t_{GW}/10^{10}$yr
n2	0.01	32	19	21	1.63	0.41	BH–BH	no	3.9×10^5
n3	0.01	22	5	9	0.0685	0.34	BH–BH	no	4.6×10^2
n6	0.01	16	1.36	4	0.0160	0.22	BH–NS	yes	5.4×10^1
n8	0.01	212	47	82	4.50	0.35	BH–BH	no	9.7×10^5
n10	0.01	135	64	80	1.37	0.92	BH–BH	no	6.6×10^1
n3	0.1	19	38	23	3.67	0.72	BH–BH	no	4.3×10^5
n7	0.1	254	38	79	0.60	0.39	BH–BH	no	3.2×10^3
n6	1.0	20	21	18	9.67	0.31	BH–BH	no	7.9×10^7
n8	1.0	5	19	8	19.3	0.15	BH–BH	yes	2.6×10^9

Column 1: run number; column 2: metallicity (Z); column 3: mass of the PCP (M_{PCP}); column 4: mass of the companion (M_{co}); column 5: chirp mass (m_c); column 6: orbital period at the end of the simulation (P_{orb}); column 7: eccentricity at the end of the simulation (e); column 8: type of binary members; column 9: status of the binary ('yes' means ejected from the YDSC, 'no' means retained); column 10: coalescence time-scale (t_{GW}) due to GW emission (Peters 1964).

($t < 4$ Myr), the situation is extremely complex. At the beginning of the simulations, the density of the YDSC is maximum (Fig. 1). The PCP, which is still building its mass through collisions, acquires companions dynamically: orbital periods $\gg$10 yr correspond to binaries that formed dynamically, often with a large eccentricity, and then become more and more bound via three-body encounters (as we see from the fact that the period decreases if the binary system survives). Some binary systems reach an extremely short period ($\ll$0.1 yr) and then disappear from the plot: these are mergers of the PCP with its companion stars. Each PCP undergoes $\sim$1 merger, on average, with one of its companion stars during the entire simulation; most of the mergers occur in the first 4 Myr, when both the PCP and the companion have not collapsed to dark remnants yet. All the mergers are triggered by three-body encounters. Binaries that disappear from Fig. 8 and do not merge split because of three-body encounters with single stars or because of SN explosions.

At $t > 4$ Myr, when the core expands and the central density of the system decreases, the situation becomes simpler. Some of the PCPs, which at $t \sim$ 3–7 Myr have become BHs (Fig. 5), were able to retain a binary companion. These binaries are stable in most cases, and survive for the entire simulation. In contrast, those PCPs that did not retain a companion after the early stages do not form stable binaries anymore, because the core density is lower.

Most importantly, all stable binaries containing a PCP are composed of two compact objects. At $Z = 0.01\ Z_\odot$ four PCPs out of ten form stable BH–BH binaries, with periods ranging from $\sim$0.07 yr to $\sim$5 yr. Two PCPs form two unstable BH–BH binaries, which break by three-body encounters before the end of the simulation. Finally, one PCP forms a stable binary with a NS, with a period of $\sim$6 d.

At $Z = 0.1\ Z_\odot$ the PCPs form two stable BH–BH binaries, with period 0.6 and 3.7 yr, respectively, plus one extremely unstable BH–BH binary. Similarly, at $Z = Z_\odot$ the PCPs form two stable BH–BH binaries, with period 9.7 and 19 yr, respectively, plus one extremely unstable BH–BH binary. At higher metallicities, the formation of stable binaries is less frequent, probably because the mass of the PCP is smaller if compared to the other objects in the YDSC. In fact, only binaries whose members are significantly more massive than the other stars are stable against dynamical exchanges with intruders (see e.g. Hills & Fullerton 1980). Moreover, at low metallicity many SNe are failed, and the BHs form without natal kick, while natal kicks tend to unbind binaries at high metallicity (see Section 3.1).

Table 2 summarizes the properties of the stable binaries at the end of the simulations.

Fig. 9 shows the mass of the companion of the PCP (M_{co}) as a function of time. In the first $\sim$4 Myr the companions are massive MS stars (with some exception of PCPs bound to low-mass MS stars) and lose mass by stellar winds. At later stages, the companions are mostly dark remnants. At $Z = Z_\odot$, the two stable binaries are composed of two BHs with masses (20,21) $M_\odot$ and (5,19) $M_\odot$ in runs n6 and n8, respectively. At $Z = 0.1\ Z_\odot$, the two stable binaries

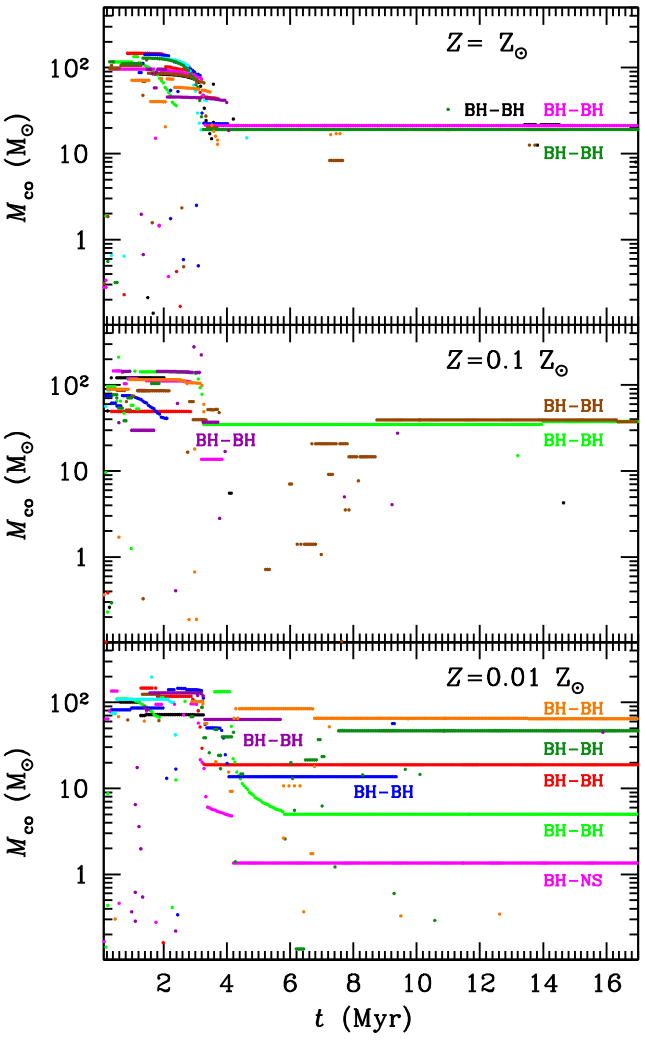

Figure 9. Mass of the companion of the PCP as a function of time, when the PCP is in a binary system. From top to bottom: $Z = Z_\odot$, $Z = 0.1\ Z_\odot$ and $Z = 0.01\ Z_\odot$. Each line is a single PCP. The labels 'BH–BH' and 'BH–NS' mark PCPs that are members of 'black hole-black hole' and 'black hole-neutron star' binaries, respectively. Colours are the same as in Fig. 8.

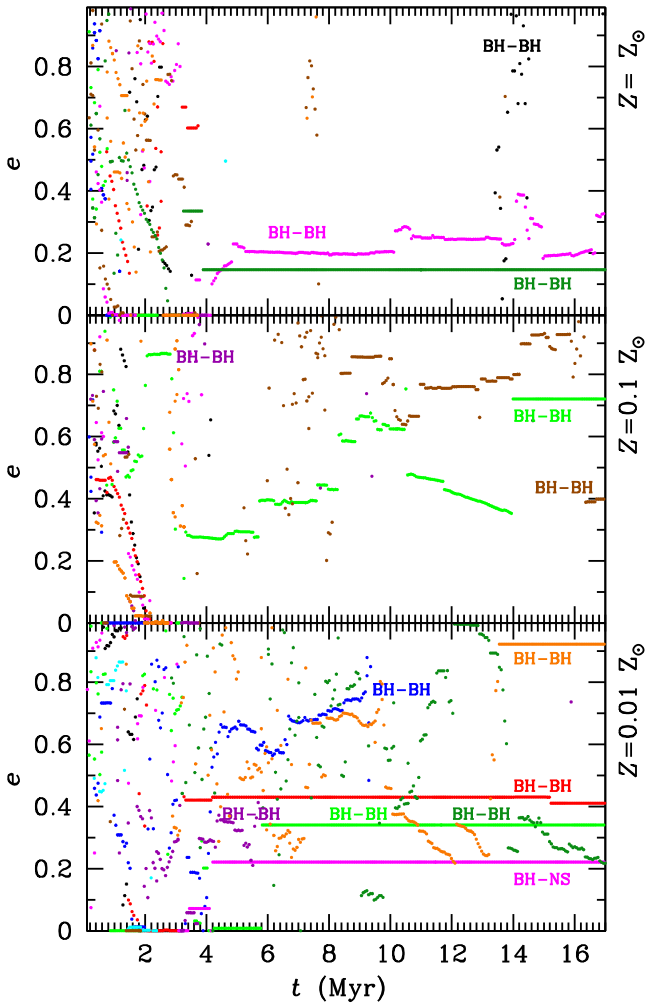

Figure 10. Eccentricity of the binary systems whose member is a PCP as a function of time. From top to bottom: $Z = Z_\odot$, $Z = 0.1\ Z_\odot$ and $Z = 0.01\ Z_\odot$. Each line is a single PCP. The labels 'BH–BH' and 'BH–NS' mark PCPs that are members of 'black hole–black hole' and 'black hole–neutron star' binaries, respectively. Colours associated with the single runs are the same as in Fig. 8.

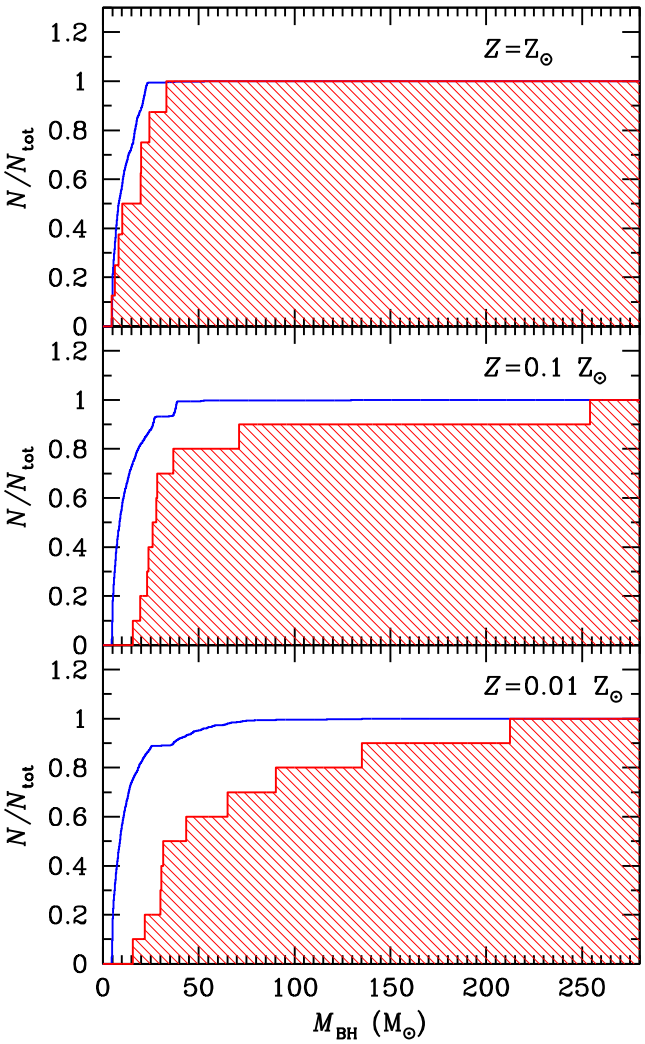

Figure 11. Cumulative mass distribution of the BHs born from the PCPs (red shaded histogram) versus the one of all BHs in the simulations (blue open histogram). From top to bottom: $Z = Z_\odot$, $Z = 0.1\ Z_\odot$ and $Z = 0.01\ Z_\odot$.

are composed of two BHs with masses (19,38) $M_\odot$ and (254,38) $M_\odot$ in runs n3 and n7, respectively. At $Z = 0.01\ Z_\odot$, we find a variety of binary masses, ranging from (16,1.36) $M_\odot$ (in the case of the BH–NS binary, run n6) to (212,47) $M_\odot$ (in run n8).

We note that three BH–BH binaries underwent an exchange in the late stages of the YDSC evolution. These are: (i) the BH–BH binary in run n10 at $Z = 0.01\ Z_\odot$ (orange line), in which M_{co} changes from 65 to 64 $M_\odot$ at $t = 13.6$ Myr; (ii) the BH–BH binary in run n3 at $Z = 0.1\ Z_\odot$ (light green line), in which M_{co} changes from 34 to 38 $M_\odot$ at $t = 14$ Myr, and (iii) the BH–BH binary in run n7 at $Z = 0.1\ Z_\odot$ (brown line), in which M_{co} changes from 39 to 38 $M_\odot$ at $t = 16.3$ Myr. In all cases, both the former and the new companions are BHs.

Fig. 10 shows the eccentricity of the PCP binaries as a function of time. The eccentricity changes very fast in many systems, even in some of the most stable PCP binaries. In case of double compact-object binaries, changes of eccentricity are entirely due to exchanges and other dynamical interactions. Highly eccentric systems are associated with recent exchanges (as in the cases of run n3 at $Z = 0.1\ Z_\odot$ and run n10 at $Z = 0.01\ Z_\odot$, see the light green line in the central panel and the orange line in the bottom panel of Figs 9 and 10, respectively), and with strong perturbations induced by an intruder (as in the case of run n7 at $Z = 0.1\ Z_\odot$, see the brown line in the central panel of Figs 9 and 10; the intruder exchanges with the companion of the PCP at the end of the simulation).

Finally, only the BH–NS binary (run n6 at $Z = 0.01\ Z_\odot$) and one of the eight BH–BH binaries (run n8 at $Z = Z_\odot$) were ejected from the parent YDSC during the simulations, while the other seven BH–BH binaries are still members of the YDSC.

3.4 Comparison with other BHs in the YDSC

As we discussed in the previous sections, most PCPs evolve into BHs. Some of them form double-compact object binaries. Is the population of BHs born from PCPs different from the rest of the BH population in the simulated YDSCs?

Fig. 11 shows the cumulative distribution of BH masses in all simulated YDSCs compared to the cumulative distribution of masses of BHs born from PCPs. The most massive BH born from a PCP is always the most massive BH for a given metallicity. The mass

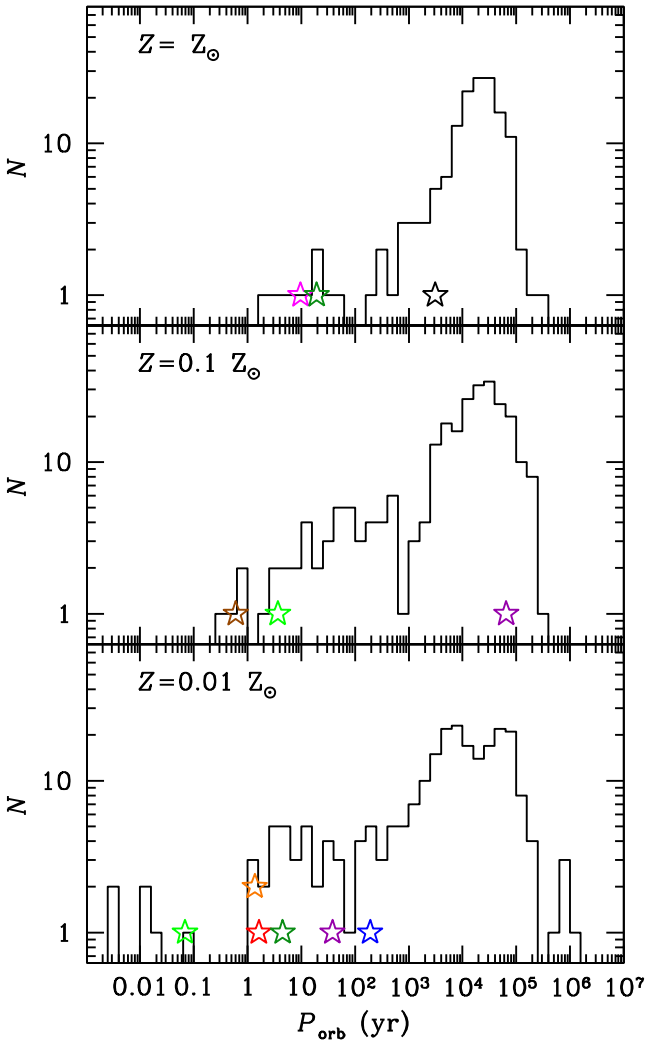

Figure 12. Distribution of minimum orbital periods of all BH–BH binaries in the simulations. Coloured stars indicate the minimum period of a BH–BH binary hosting a PCP (colours are the same as in Fig. 8). From top to bottom: $Z = Z_{\odot}$, $Z = 0.1\ Z_{\odot}$ and $Z = 0.01\ Z_{\odot}$.

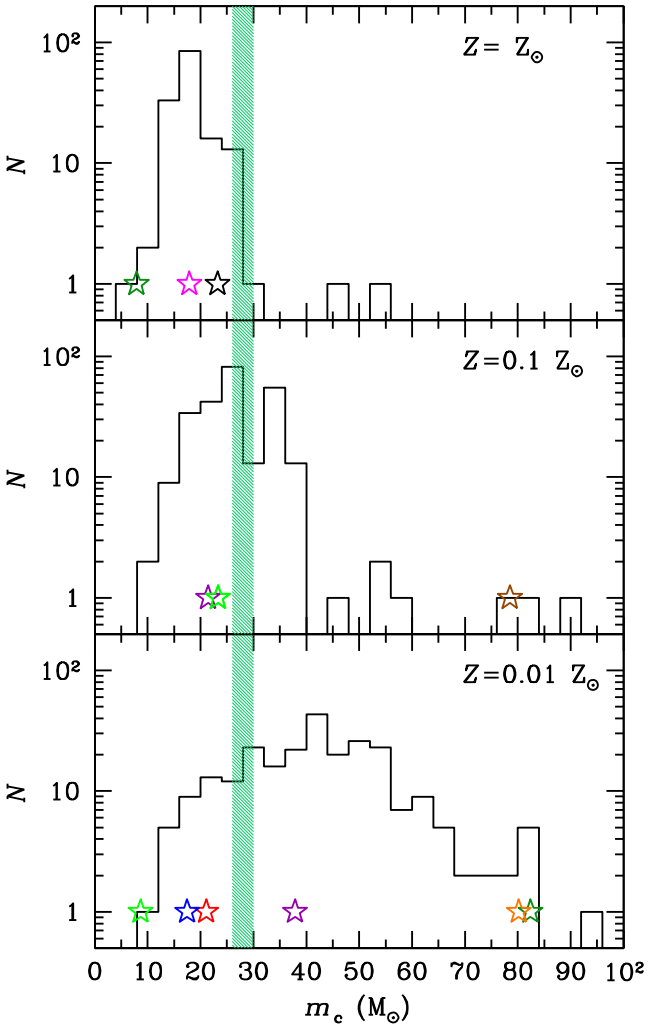

Figure 13. Distribution of chirp masses (m_c) of all BH–BH binaries in the simulations. Most of these binaries are unstable. Coloured stars indicate the final chirp mass of a BH–BH binary hosting a PCP (colours are the same as in Fig. 12). The shaded green area is the measured chirp mass of GW150914 (Abbott et al., 2016a). From top to bottom: $Z = Z_{\odot}$, $Z = 0.1\ Z_{\odot}$ and $Z = 0.01\ Z_{\odot}$.

distribution of BHs born from PCPs is significantly skewed towards higher masses than the distribution of all BHs. The Kolmogorov–Smirnov (KS) test probability that the overall BH distribution and the distribution of BHs born from PCPs are drawn from the same population is 3×10^{-5}, 3×10^{-4} and 10^{-3} for $Z = 0.01$, 0.1 and 1 $Z_{\odot}$, respectively. Thus, the three distributions are significantly different.

Many BH–BH binaries form in the simulated YDSCs dynamically: 246, 257 and 153 BH–BH binaries at $Z = 0.01$, 0.1 and 1 $Z_{\odot}$ (the efficiency is lower at solar metallicity because of the smaller average BH masses). Fig. 12 compares the distribution of the minimum orbital period of all simulated BH–BH binaries with the orbital periods of BH–BH binaries that host a PCP. Most BH–BH binaries are extremely soft, i.e. their orbital period is extremely long for the entire simulation. As already shown by Ziosi et al. (2014), such soft BH–BH binaries have short lifetimes, and continuously break and change members by dynamical exchanges. The shortest period of a BH–BH binary at low metallicity is ∼100 times shorter than the shortest period at high metallicity. The stable BH–BH binaries that contain a PCP are among the BH–BH binaries with the shortest period, at all metallicities.

Fig. 13 shows the distribution of the chirp mass of the BH–BH binaries, defined as $m_c = (m_1\, m_2)^{3/5}(m_1 + m_2)^{-1/5}$, where m_1 and m_2 are the masses of the two components of the binary. The chirp mass is particularly important for GWs, since it determines how fast the binary sweeps, or chirps, through a frequency band (the amplitude and the frequency of GWs scale as $m_c^{5/3}$ and $m_c^{-5/8}$, respectively). The distribution of chirp masses strongly depends on the metallicity, as a consequence of the assumed recipes for BH formation. We note that several PCP binaries have relatively small chirp masses, and do not differ from the rest of the sample.

4 DISCUSSION

4.1 Predictions for gravitational wave events

The first direct detection of GWs was recently reported by Abbott et al. (2016b). The signal has been interpreted as emitted by a

merging BH–BH binary with masses (36^{+5}_{-4}, 29^{+4}_{-4}) $M_\odot$ (The LIGO Scientific Collaboration & the Virgo Collaboration 2016). Previous studies already predicted the existence of such massive stellar BHs (e.g. Mapelli et al. 2009; Belczynski et al. 2010; Spera et al. 2015). However, it is difficult that an isolated binary system composed of two massive stars evolves into a BH–BH binary with such massive BHs (e.g. Linden et al. 2010), because mass transfer and common envelope often lead to the merger of the two stars or to the loss of most of the initial mass of the system.

In YDSCs, a massive BH–BH binary might form from dynamical exchanges (Ziosi et al. 2014). In this case, the two massive BHs did not originate in the same primordial binary, but they entered the same binary as a consequence of dynamical exchanges with other stars.

Ziosi et al. (2014) find that most BH–BH mergers in YDSCs are expected to occur between low-mass BHs (5–15 $M_\odot$), despite the efficiency of dynamical exchanges (see also O'Leary et al. 2006; Sadowski et al. 2008; Downing et al. 2010, 2011; Clausen, Sigurdsson & Chernoff 2013; Morscher et al. 2015; Rodriguez et al. 2015; Amaro-Seoane & Chen 2016; Chatterjee, Rodriguez & Rasio 2016; O'Leary, Meiron & Kocsis 2016 for other predictions). The YDSCs simulated by Ziosi et al. (2014) have initial mass ∼3500 $M_\odot$ (i.e. about 20 times less massive than the YDSCs we simulated). Do the results of Ziosi et al. (2014) still hold in more massive and denser YDSCs?

In the previous section, we reported that several PCPs form stable BH–BH or even BH–NS binaries in the simulated YDSCs. Two of such binaries have masses similar to the merging binary system that was recently detected by Advanced LIGO. These are system n2 at $Z = 0.01$ $Z_\odot$ and system n3 at $Z = 0.1$ $Z_\odot$, which have mass (32,19) and (38,19) $M_\odot$, respectively.

We now estimate the coalescence time-scale for such PCP binaries as well as for the other BH–BH binaries in the simulations. We define the coalescence time-scale as the time for the semimajor axis of a binary to sink to zero, due to the emission of GWs (Peters 1964)

$$t_{\rm GW} = \frac{5}{256}\,\frac{c^5\,a^4\,(1-e^2)^{7/2}}{G^3\,m_1\,m_2\,(m_1+m_2)}, \qquad (4)$$

where c is the speed of light, G is the gravitational constant, a and e are the semimajor axis and the eccentricity of the binary system composed of two objects with mass m_1 and m_2.

Fig. 14 shows $t_{\rm GW}$ for the simulated BH binary systems that are closest to coalescence, including the nine stable PCP binaries in Table 2. Apart from the BH–NS binary already discussed in this paper, all the other systems are BH–BH binaries, indicating that the formation of BH–NS binaries is extremely rare if primordial binaries are not included. For the same reason, we decided not to include the statistics of NS-NS binaries. Ziosi et al. (2014) recently showed that nearly all NS-NS binaries come from primordial binaries, even in YDSCs.

All but one simulated double-compact object systems are not expected to coalesce within a Hubble time. The only BH–BH binary that is expected to coalesce within the Hubble time (with $t_{\rm GW} \sim$ 1.2 Gyr) is at low metallicity ($Z = 0.01$ $Z_\odot$) and has a mass of (17,16) $M_\odot$, a minimum orbital period $P_{\rm orb} \sim 1.3$ d and an eccentricity $e \sim 0.061$. There is a clear trend with metallicity: the BH systems with the shorter $t_{\rm GW}$ are in metal-poor YDSCs. The reason is that metal-poor YDSCs host more massive BHs (which are more efficient in acquiring companions through dynamical interactions, Ziosi et al. 2014).

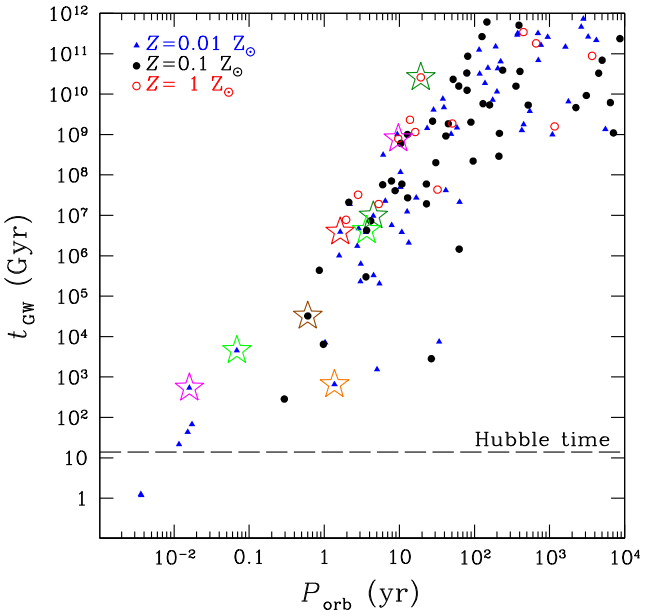

Figure 14. Coalescence time-scale of BH–BH and BH–NS binaries in the simulated YDSCs as a function of their orbital period. Most simulated BH binaries are not shown in this plot because they have $t_{\rm GW} > 10^{12}$ Gyr or $P_{\rm orb} > 10^4$ yr. Blue solid triangles: BH binaries at $Z = 0.01$ $Z_\odot$; black solid circles: BH binaries at $Z = 0.1$ $Z_\odot$; red open circles: BH binaries at $Z = Z_\odot$. The nine stars mark the position of the eight stable BH–BH binaries and of the NS-BH binary that contain a PCP (colours are the same as in Fig. 2). The horizontal black dashed line corresponds to the Hubble time.

All nine stable PCP binaries are among the systems with the shortest $t_{\rm GW}$, but they are not expected to merge within a Hubble time. It must be said, however, that the orbital properties of these binaries are expected to change if they remain in the YDSC after the end of the simulation. Three-body encounters (especially exchanges) can further reduce the semimajor axis and increase the eccentricity, leading to a decrease of $t_{\rm GW}$, too. For example, from Fig. 8 it is apparent that the period of several BH–BH binaries is still decreasing because of three-body encounters and dynamical exchanges. In this paper, we chose to stop the simulations at $t =$ 17 Myr because we did not add any prescription for the tidal field of the host galaxy and we cannot account for tidal evaporation of the YDSC. In a forthcoming study, we will add recipes for the tidal field of the host galaxy.

Our results seem to confirm the main finding of Ziosi et al. (2014): while most BH–BH binaries (and especially the most massive BH–BH binaries) in YDSCs form from dynamical exchanges, it is difficult that dynamically formed systems merge within a Hubble time, even if they host the product of runaway collisions. Our result holds if YDSCs live for $<10^8$ Myr. Thus, the time when YDSCs are disrupted in the tidal field of the host galaxy is important. However, we must stress that the simulated sample (30 YDSCs) is statistically small. Using the same formalism as in equation 3 of Ziosi et al. (2014), the predicted merger rate of the simulated BH–BH systems is

$$R_{\rm BH-BH} \sim 10^{-3}\,{\rm Mpc^{-3}\,Myr^{-1}} \left(\frac{n_{\rm merg}}{1}\right) \left(\frac{2\times10^6\,M_\odot}{M_*}\right) \left(\frac{1.2\,{\rm Gyr}}{t_{\rm GW}}\right) \left(\frac{t_{\rm life}}{10^8\,{\rm yr}}\right) \left(\frac{\rho_{\rm SFR}}{0.015\,M_\odot\,{\rm yr^{-1}\,Mpc^{-3}}}\right), \qquad (5)$$

where $n_{\rm merg}$ is the number of BH–BH systems that merge in a Hubble time in our simulations, $t_{\rm GW}$ is the maximum coalescence time of such systems, M_* is the total simulated stellar mass (given by the number of simulated YDSCs multiplied by their mass), $t_{\rm life}$ is the lifetime of an YDSC, and $\rho_{\rm SFR}$ is the cosmic star formation rate density at low redshift (Hopkins & Beacom 2006). Since the instrumental range of Advanced LIGO and Virgo for BH–BH binaries with chirp mass $m_{\rm c} \sim 15$ M$_\odot$ is $\sim$1 Gpc, equation (5) leads to a detection rate $\approx$4 yr^{-1}.

The minimum merger rate derived from the LIGO detection is $\sim 2 \times 10^{-3}$ Mpc^{-3} Myr^{-1} (The LIGO Scientific Collaboration & the Virgo Collaboration 2016), i.e. similar to (and slightly higher than) what we found. However, the merger rate we obtain in equation (5) should be taken as a strong lower limit, because we neglect the contribution of primordial binaries. To get more accurate estimates, we need a larger simulation sample, and we must include primordial binaries.

To conclude, we point out that the most massive BH–BH binaries and the best merger candidates are at metallicity $Z = 0.01$ Z$_\odot$. This metallicity is typical of old Milky Way globular clusters. If the properties of globular clusters in the early stages of their evolution were similar to the properties of YDSCs in the nearby Universe, this means that the most massive BH–BH binaries formed in globular clusters. These massive BH–BH binaries born in globular clusters can give an important contribution to detectable GW signal.

4.2 Comparison with other scenarios of IMBH formation

The runaway merger scenario is one of the principal mechanisms that were proposed to form IMBHs. Other popular scenarios of IMBH formation are the direct collapse of very massive (>250 M$_\odot$) Population III stars (Madau & Rees 2001; Schneider et al. 2002; Heger et al. 2003), and the repeated mergers of stellar-mass BHs with stars and other BHs, triggered by dynamical interactions in star clusters (Miller & Hamilton 2002; Giersz et al. 2015).

Both the latter model and the runaway merger scenario rely on the importance of dynamical interactions to trigger the formation of IMBHs. The main difference between these two models is the formation time-scale: the runaway merger occurs very fast (mostly before the collapse of the PCP into a BH), while the scenario of repeated mergers involves objects that have already collapsed to BHs. However, the distinction between these two models is rather weak, since even in the runaway merger scenario an IMBH can keep growing through mergers with other BHs after its formation. For example, Giersz et al. (2015) note that, in their simulations, there is a transition between a first epoch of fast formation of IMBHs by collisions (at the beginning of cluster evolution) and a second epoch (at $t \gtrsim 3$ Gyr) of slower build-up of IMBHs by dynamical encounters involving binary systems. Our results are reminiscent of the epoch of fast IMBH formation described in Giersz et al. (2015), while the fact that our simulated IMBHs tend to form binaries with other BHs suggests that they might undergo more binary interactions at later times, as studied by Giersz et al. (2015).

In contrast, IMBHs formed by the collapse of metal-free stars at high redshift are not expected to be in star clusters nowadays. As shown by previous studies (Mapelli, Ferrara & Rea 2006; Kuranov et al. 2007; Mapelli 2007), it is very unlikely for these Population III IMBHs to acquire a companion and to be observed as sources of X-ray emission or GWs.

4.3 Caveats and future work

Unraveling the runaway merger in YDSCs is an arduous task, because it involves a plethora of astrophysical processes (e.g. dynamical friction, mass segregation, dynamics of three-body encounters, stellar and binary evolution, hydrodynamics of collisions, BH formation, structural star cluster evolution), that occur on considerably different scales (from the stellar radius up to several parsecs). Hence, many approximations and assumptions were needed, in order to make our simulations feasible. In this section, we discuss the main issues of these approximations.

We assumed that the entire mass of two colliding objects (either stars of BHs) ends up into the collision product. Hydrodynamical simulations of the collision of massive stars indicate that mass-losses can be of the order of $\sim$25 per cent of the entire mass of the merger product. Moreover, if the two colliding objects are a star and a BH, less than 50 per cent of the incoming star mass might be directly accreted on to the BH (see e.g. Ramirez-Ruiz & Rosswog 2009; Guillochon & Ramirez-Ruiz 2013). This implies that the maximum masses of PCPs shown in our Fig. 5 are overestimated. This issue is particularly sensitive for collisions of stars with BHs, because the collision product does not undergo further mass-loss by stellar winds. In their Monte Carlo simulations, Giersz et al. (2015) compare simulations where 100 per cent and 25 per cent of the mass of the colliders end up in the collision product, respectively. When only 25 per cent of the mass is accreted on to the collision product, the final mass is significantly lower, but IMBH formation is still possible (see fig. 7 of Giersz et al. 2015).

To evolve the most massive stars, we extend the fitting formulate of Hurley et al. (2000) to masses >100 M$_\odot$. While we use PARSEC stellar evolution tracks to check that the radii do not become unphysical (Bressan et al. 2012; Tang et al. 2014; Chen et al. 2015), this assumption is not self-consistent. In future, we plan to use up-to-date PARSEC stellar evolution tracks for all stars (Spera et al., in preparation). Moreover, we used an old prescription for stellar rejuvenation (Portegies Zwart et al. 1999), which should be updated accounting for chemical mixing.

No primordial binaries are included in our simulations. The reason is that integrating binaries is the bottleneck of direct N-body simulations, but we know that a high binary fraction is observed in young star clusters (e.g. Li et al. 2013). If there are no primordial binaries, binaries can form through dynamical encounters. This mechanism is efficient in our simulations (see Fig. 1), thanks to the high central density, but the absence of primordial binaries has an impact on our results. Mapelli et al. (2013) and Mapelli & Zampieri (2014) study the effect of different primordial binary fractions on the demographics of BH binaries (defined as binaries hosting at least one BH) in YDSCs with mass $M_{\rm TOT} \sim 3500$ M$_\odot$, i.e. 20 times smaller than the YDSCs we simulate here. They assume that 0, 18 and 33 per cent of stars are members of primordial binaries in their simulations, and find that the number of BH binaries born from a dynamical exchange does not depend on the primordial binary fraction, whereas the number of BH binaries born from primordial binaries scales almost linearly with the primordial binary fraction. This implies that our merger rate of BH–BH binaries is a strong lower limit. Moreover, Monte Carlo simulations (Giersz et al. 2015; Leigh et al. 2015), where a high fraction of primordial binaries can be accounted for, indicate that binary interactions are important for the build-up of IMBHs, by enhancing stellar collisions.

Finally, our initial conditions do not account for the effects of gas from the parent molecular cloud. Leigh et al. (2014) suggest that gas damping (i.e. the contribution of gas to dynamical friction) can

accelerate mass segregation and even lead to cluster contraction. This might enhance the stellar collisions leading to the runaway merger. On the other hand, a relatively fast gas expulsion due to stellar winds and SN explosions can lead to the expansion of the cluster (Marks, Kroupa & Baumgardt 2008; Marks et al. 2012; Leigh et al. 2013), reducing the efficiency of stellar collisions. This effect is evident also in our simulations: we do not include the gas of the parent molecular cloud, but mass-loss by SNe and stellar winds leads to a significant expansion of the cluster, associated with a decrease of the total binary binding energy (Fig. 1). In a forthcoming study, we will account for the influence of gas on the early stages of the YDSC evolution.

5 CONCLUSIONS

We investigated the runaway collision scenario by means of direct *N*-body simulations of YDSCs ($N_* = 10^5$ particles) with three different metallicities: 0.01, 0.1 and 1 $Z_\odot$. We ran 10 realizations of the same YDSC per each metallicity, adopting a King model (King 1966), with virial radius $r_v = 1$ pc and dimensionless central potential $W_0 = 9$. Stellar masses are distributed according to a Kroupa (2001) initial mass function.

We assume no mass-loss during the collision of two stars. Thus, the mass of the merger product immediately after each collision should be considered as an upper limit. Moreover, we do not include primordial binaries, which might enhance stellar collisions, and we do not account for the influence of the relic gas from the parent molecular cloud.

On the other hand, we adopt realistic prescriptions for the stellar winds (Mapelli et al. 2013). Thus, we model mass-loss by stellar winds self-consistently, and we account for the impact of this mass-loss on subsequent collisions of each merger product with other stars, whereas previous studies (e.g. Glebbeek et al. 2009) included realistic stellar winds only *a posteriori*, in *N*-body simulations that were run without stellar evolution.

The maximum mass that a PCP can achieve in our simulations is close to $\sim$500 $M_\odot$, regardless of the metallicity. The maximum mass of the PCP is sensitive to the number of collisions and to the time when the first collision occurs. In contrast, the final mass of the PCP (when it becomes a stellar remnant) does not depend on the number of collisions and on the time of the first collision. The mass of the PCP remnant is affected by the metallicity of the progenitor stars, because stellar winds depend on metallicity.

BHs with mass up to $\sim$250 $M_\odot$ form from the direct collapse of a PCP, if the metallicity is sufficiently low ($Z \leq 0.1\ Z_\odot$) and if the central density of the YDSC is sufficiently high (i.e. in the first $\sim$5 Myr of the YDSC evolution). Four BHs born from PCPs have mass $\gtrsim 90\ M_\odot$, and can be considered genuine IMBHs. Moreover, if the metallicity is low ($Z \leq 0.1\ Z_\odot$), massive stellar BHs ($25 \leq m_{\rm BH}/M_\odot \leq 90$) can form from the direct collapse of a massive star, even without runaway collisions.

We find that $\sim$60 per cent of the simulated PCPs are not ejected from their parent YDSC for the entire simulation. Most PCPs acquire companions through dynamical interactions. In the first $\sim$4 Myr, PCP binaries are short-lived: they are continuously destroyed by collisions, SN explosions and dynamical interactions. Those PCP binaries that remain bound after this early stage survive for the entire simulation. At the end of the simulations ($t = 17$ Myr), all stable PCP binaries are double-compact object binaries. We find nine stable PCP binaries: eight of them are BH–BH binaries, and one is a BH–NS binary.

Five of the nine stable PCP binaries (including the BH–NS binary) form at $Z = 0.01\ Z_\odot$. Among the other four systems, two BH–BH binaries are at $Z = 0.1\ Z_\odot$ and two are at $Z = Z_\odot$. We suggest that double-compact object formation is more efficient at low metallicity, because the remnant mass is higher (massive objects are favoured in acquiring companions dynamically, Hills 1991).

The periods of the stable double-compact object PCP binaries range from few days up to $\sim$20 years. Their eccentricities range from 0.15 to 0.92. High eccentricities are associated with recent exchanges and with strong perturbations induced by intruders. The masses of the primary members range from $\sim$15 $M_\odot$ to $\sim$250 $M_\odot$ (Table 2). Two of these binaries have masses similar to the merging BH–BH binary system recently detected by Advanced LIGO. These are system n2 at $Z = 0.01\ Z_\odot$ and system n3 at $Z = 0.1\ Z_\odot$, which have mass (32,19) and (38,19) $M_\odot$, respectively. In comparison with other simulated BH–BH binaries (those that do not contain the PCPs), the PCP binaries have relatively short periods.

The merger rate of simulated BH–BH binaries is $\sim 10^{-3}$ Mpc^{-3} Myr^{-1}, corresponding to $\sim$4 expected detections per year by Advanced LIGO and Virgo. This predicted rate should be taken as a strong lower limit, because we neglect the contribution of primordial binaries. None of the stable PCP binaries is expected to merge in a Hubble time. Increasing the statistics of simulated YDSCs and adding a conspicuous fraction of primordial binaries are essential steps to make more accurate predictions for the detection of GWs from PCP binary mergers.

ACKNOWLEDGEMENTS

I thank the referee, Mirek Giersz, for his accurate reading of the manuscript and for the numerous comments that improved this work significantly. I also thank Alessandro Bressan, Alessandro Trani, Emanuele Ripamonti, Marica Branchesi, Mario Spera, Ugo Niccolò Di Carlo, Enrico Montanari and Andrea Moretti for useful discussions. I made use of the STARLAB (ver. 4.4.4) public software environment and of the SAPPORO library (Gaburov, Harfst & Portegies Zwart 2009). I thank the developers of STARLAB, and especially its primary authors (P. Hut, S. McMillan, J. Makino, and S. Portegies Zwart). I thank the authors of SAPPORO, and in particular E. Gaburov, S. Harfst, and S. Portegies Zwart. I acknowledge the CINECA Award N. HP10C3ANJY (VMStars) for the availability of high performance computing resources and support. The simulations were run on the graphics processing unit (GPU) cluster EURORA at CINECA. I acknowledge financial support from the Italian Ministry of Education, University and Research (MIUR) through grant FIRB 2012 RBFR12PM1F, from INAF through grant PRIN-2014-14, and from the MERAC Foundation.

REFERENCES

Abbott B. P. et al., 2016a, ApJ, 818, L22
Abbott B. P. et al., 2016b, Phys. Rev. Lett., 116, 061102
Amaro-Seoane P., Chen X., 2016, MNRAS, 458, 3075
Arca-Sedda M., 2016, MNRAS, 455, 35
Banerjee S., Kroupa P., Oh S., 2012, MNRAS, 426, 1416
Belczynski K., Bulik T., Fryer C. L., Ruiter A., Valsecchi F., Vink J. S., Hurley J. R., 2010, ApJ, 714, 1217
Bressan A., Marigo P., Girardi L., Salasnich B., Dal Cero C., Rubele S., Nanni A., 2012, MNRAS, 427, 127
Chatterjee S., Rodriguez C. L., Rasio F. A., 2016, preprint (arXiv: 1603.00884)
Chen Y., Bressan A., Girardi L., Marigo P., Kong X., Lanza A., 2015, MNRAS, 452, 1068

Clausen D., Sigurdsson S., Chernoff D. F., 2013, MNRAS, 428, 3618
Colgate S. A., 1967, ApJ, 150, 163
Crowther P. A., Schnurr O., Hirschi R., Yusof N., Parker R. J., Goodwin S. P., Kassim H. A., 2010, MNRAS, 408, 731
de Kool M., 1990, ApJ, 358, 189
Downing J. M. B., Benacquista M. J., Giersz M., Spurzem R., 2010, MNRAS, 407, 1946
Downing J. M. B., Benacquista M. J., Giersz M., Spurzem R., 2011, MNRAS, 416, 133
Ebisuzaki T. et al., 2001, ApJ, 562, L19
Freitag M., Rasio F. A., Baumgardt H., 2006a, MNRAS, 368, 121
Freitag M., Gürkan M. A., Rasio F. A., 2006b, MNRAS, 368, 141
Fryer C. L., 1999, ApJ, 522, 413
Fryer C. L., Kalogera V., 2001, ApJ, 554, 548
Fryer C. L., Belczynski K., Wiktorowicz G., Dominik M., Kalogera V., Holz D. E., 2012, ApJ, 749, 91
Gaburov E., Lombardi J. C., Portegies Zwart S., 2008a, MNRAS, 383, L5
Gaburov E., Gualandris A., Portegies Zwart S., 2008b, MNRAS, 384, 376
Gaburov E., Harfst S., Portegies Zwart S., 2009, New Astron., 14, 630
Gaburov E., Lombardi J. C. Jr, Portegies Zwart S., 2010, MNRAS, 402, 105
Gieles M., Portegies Zwart S. F., 2011, MNRAS, 410, L6
Giersz M., Leigh N., Hypki A., Lützgendorf N., Askar A., 2015, MNRAS, 454, 3150
Glebbeek E., Gaburov E., de Mink S. E., Pols O. R., Portegies Zwart S. F., 2009, A&A, 497, 255
Glebbeek E., Gaburov E., Portegies Zwart S., Pols O. R., 2013, MNRAS, 434, 3497
Goswami S., Umbreit S., Bierbaum M., Rasio F. A., 2012, ApJ, 752, 43
Guillochon J., Ramirez-Ruiz E., 2013, ApJ, 767, 25
Gürkan M. A., Freitag M., Rasio F. A., 2004, ApJ, 604, 632
Gürkan M. A., Fregeau J. M., Rasio F. A., 2006, ApJ, 640, L39
Hamann W.-R., Koesterke L., 1998, A&A, 335, 1003
Hartman J. W., 1997, A&A, 322, 127
Heger A., Fryer C. L., Woosley S. E., Langer N., Hartmann D. H., 2003, ApJ, 591, 288
Heggie D. C., 1975, MNRAS, 173, 729
Hills J. G., 1976, MNRAS, 175, 1P
Hills J. G., 1989, AJ, 97, 222
Hills J. G., 1991, AJ, 102, 704
Hills J. G., 1992, AJ, 103, 1955
Hills J. G., Fullerton L. W., 1980, AJ, 85, 1281
Hopkins A. M., Beacom J. F., 2006, ApJ, 651, 142
Humphreys R. M., Davidson K., 1994, PASP, 106, 1025
Hurley J. R., Pols O. R., Tout C. A., 2000, MNRAS, 315, 543
King I. R., 1966, AJ, 71, 64
Kroupa P., 2001, MNRAS, 322, 231
Kudritzki R. P., 2002, ApJ, 577, 389
Kudritzki R. P., Pauldrach A., Puls J., 1987, A&A, 173, 293
Kuranov A. G., Popov S. B., Postnov K. A., Volonteri M., Perna R., 2007, MNRAS, 377, 835
Lada C. J., Lada E. A., 2003, ARA&A, 41, 57
Leigh N., Giersz M., Webb J. J., Hypki A., De Marchi G., Kroupa P., Sills A., 2013, MNRAS, 436, 3399
Leigh N. W. C., Mastrobuono-Battisti A., Perets H. B., Böker T., 2014, MNRAS, 441, 919
Leigh N. W. C., Giersz M., Marks M., Webb J. J., Hypki A., Heinke C. O., Kroupa P., Sills A., 2015, MNRAS, 446, 226
Li C., de Grijs R., Deng L., 2013, MNRAS, 436, 1497
Linden T., Kalogera V., Sepinsky J. F., Prestwich A., Zezas A., Gallagher J. S., 2010, ApJ, 725, 1984
MacLeod M., Trenti M., Ramirez-Ruiz E., 2016, ApJ, 819, 70
Madau P., Rees M. J., 2001, ApJ, 551, L27
Makino J., Aarseth S. J., 1992, PASJ, 44, 141
Mapelli M., 2007, MNRAS, 376, 1317
Mapelli M., Bressan A., 2013, MNRAS, 430, 3120
Mapelli M., Zampieri L., 2014, ApJ, 794, 7
Mapelli M., Ferrara A., Rea N., 2006, MNRAS, 368, 1340
Mapelli M., Colpi M., Zampieri L., 2009, MNRAS, 395, L71
Mapelli M., Ripamonti E., Zampieri L., Colpi M., Bressan A., 2010, MNRAS, 408, 234
Mapelli M., Zampieri L., Ripamonti E., Bressan A., 2013, MNRAS, 429, 2298
Marks M., Kroupa P., Baumgardt H., 2008, MNRAS, 386, 2047
Marks M., Kroupa P., Dabringhausen J., Pawlowski M. S., 2012, MNRAS, 422, 2246
Meurs E. J. A., van den Heuvel E. P. J., 1989, A&A, 226, 88
Miller M. C., Hamilton D. P., 2002, MNRAS, 330, 232
Moeckel N., Clarke C. J., 2011, MNRAS, 410, 2799
Morscher M., Pattabiraman B., Rodriguez C., Rasio F. A., Umbreit S., 2015, ApJ, 800, 9
Muijres L., Vink J. S., de Koter A., Hirschi R., Langer N., Yoon S.-C., 2012, A&A, 546, A42
O'Leary R. M., Rasio F. A., Fregeau J. M., Ivanova N., O'Shaughnessy R., 2006, ApJ, 637, 937
O'Leary R. M., Meiron Y., Kocsis B., 2016, preprint (arXiv:1602.02809)
Pan T., Loeb A., Kasen D., 2012, MNRAS, 423, 2203
Peters P. C., 1964, Phys. Rev., 136, 1224
Portegies Zwart S. F., McMillan S. L. W., 2002, ApJ, 576, 899
Portegies Zwart S. F., van den Heuvel E. P. J., 2007, Nature, 450, 388
Portegies Zwart S. F., Verbunt F., 1996, A&A, 309, 179
Portegies Zwart S. F., Makino J., McMillan S. L. W., Hut P., 1999, A&A, 348, 117
Portegies Zwart S. F., McMillan S. L. W., Hut P., Makino J., 2001, MNRAS, 321, 199
Portegies Zwart S. F., Baumgardt H., Hut P., Makino J., McMillan S. L. W., 2004, Nature, 428, 724
Portegies Zwart S. F., McMillan S. L. W., Gieles M., 2010, ARA&A, 48, 431
Quinlan G. D., Shapiro S. L., 1990, ApJ, 356, 483
Ramirez-Ruiz E., Rosswog S., 2009, ApJ, 697, L77
Rodriguez C. L., Morscher M., Pattabiraman B., Chatterjee S., Haster C.-J., Rasio F. A., 2015, Phys. Rev. Lett., 115, 051101
Sadowski A., Belczynski K., Bulik T., Ivanova N., Rasio F. A., O'Shaughnessy R., 2008, ApJ, 676, 1162
Sanders R. H., 1970, ApJ, 162, 791
Schneider R., Ferrara A., Natarajan P., Omukai K., 2002, ApJ, 571, 30
Spera M., Mapelli M., Bressan A., 2015, MNRAS, 451, 4086
Tang J., Bressan A., Rosenfield P., Slemer A., Marigo P., Girardi L., Bianchi L., 2014, MNRAS, 445, 4287
The LIGO Scientific Collaboration the Virgo Collaboration 2016, preprint (arXiv:1602.03840)
Trani A. A., Mapelli M., Bressan A., 2014, MNRAS, 445, 1967
van den Heuvel E. P. J., Portegies Zwart S. F., 2013, ApJ, 779, 114
Vink J. S., de Koter A., 2005, A&A, 442, 587
Vink J. S., de Koter A., Lamers H. J. G. L. M., 2001, A&A, 369, 574
Webbink R. F., 1984, ApJ, 277, 355
Yungelson L. R., van den Heuvel E. P. J., Vink J. S., Portegies Zwart S. F., de Koter A., 2008, A&A, 477, 223
Ziosi B. M., Mapelli M., Branchesi M., Tormen G., 2014, MNRAS, 441, 3703

APPENDIX A: OTHER COLLISION PRODUCTS

In this appendix, we summarize the properties of the other collision products that form after the PCP (hereafter, other collision products, OCPs). Fig. A1 shows the masses of the OCPs and of the BHs born from the OCPs.

All the OCPs but two undergo a single collision during the entire simulation. No OCP undergoes more than two collisions. This is a striking difference with the PCPs, most of which undergo multiple collisions. The maximum mass of the OCPs is always the same as the mass after the first collision (m_{1st}).

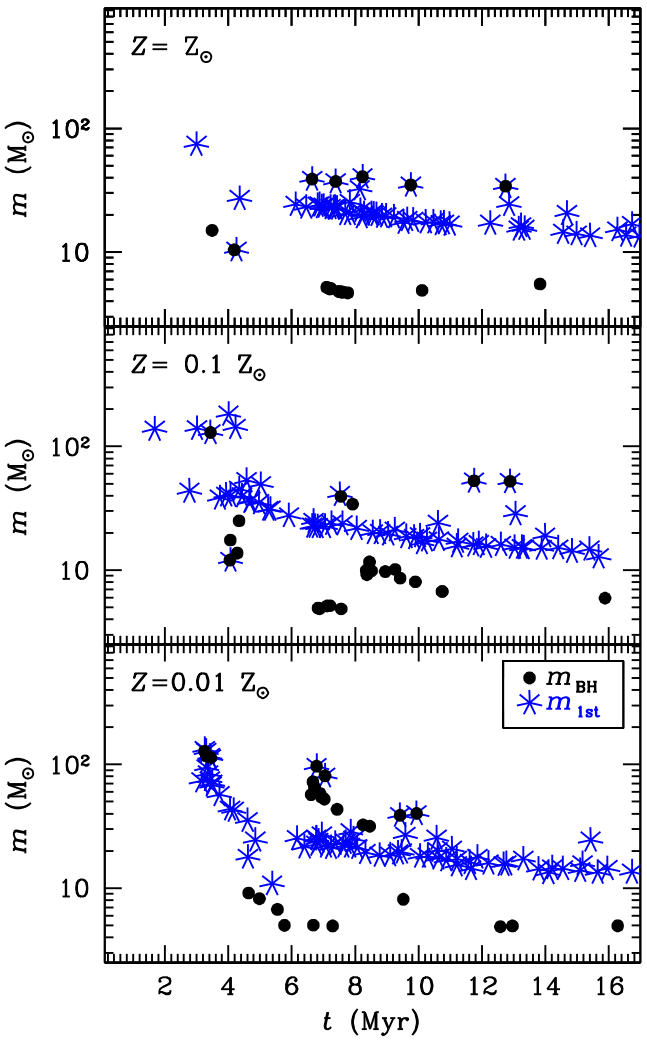

Figure A1. Mass of the OCP after the first collision (m_{1st}, blue asterisks), and mass of the BH born from the OCP (m_{BH}, black solid circles) as a function of time for solar metallicity (top), $Z = 0.1\ Z_\odot$ (centre) and $Z = 0.01\ Z_\odot$ (bottom).

Fig. A1 shows that the maximum mass of OCPs is always $<200\ M_\odot$, and most OCPs have mass $\ll 100\ M_\odot$. In general, the PCP is the most massive object in the star cluster. Moreover, the collision that leads to the formation of the first OCP is significantly delayed with respect to the formation of the PCP: all OCPs but three form at $t > 3$ Myr.

Despite this, some massive BHs form also from the collapse of the OCPs. Among the dark remnants born from the OCPs, three BHs at $Z = 0.01\ Z_\odot$ and one BH at $Z = 0.1\ Z_\odot$ have mass $>100\ M_\odot$.

In our simulations, we find 69, 58, and 53 OCPs at $Z = 0.01$, 0.1 and 1 $Z_\odot$, respectively. Only 26, 25 and 19 of these OCPs become BHs at $Z = 0.01$, 0.1 and 1 $Z_\odot$, respectively. These represent only the ∼1.0–1.5 per cent of all the BHs in the simulations (the total number of BHs in our simulations is 1689, 1746 and 1713 at $Z = 0.01$, 0.1 and 1 $Z_\odot$, respectively). The mass of the other OCPs is too small to form a BH. Binary interactions are of primary importance for the formation of OCPs as they were for the formation of the PCP. This is consistent with previous results by e.g. Gaburov et al. (2008b) and Giersz et al. (2015).

This paper has been typeset from a TEX/LATEX file prepared by the author.